VIP Metal Oxide Catalysts Very Important Paper

DOI: 10.1002/anie.201404208

A Reliable Aerosol-Spray-Assisted Approach to Produce and Optimize Amorphous Metal Oxide Catalysts for Electrochemical Water Splitting**

*Long Kuai, Jing Geng, Changyu Chen, Erjie Kan, Yadong Liu, Qing Wang, and Baoyou Geng**

Abstract: *An aerosol-spray-assisted approach (ASAA) is proposed and confirmed as a precisely controllable and continuous method to fabricate amorphous mixed metal oxides for electrochemical water splitting. The proportion of metal elements can be accurately controlled to within (5±5) %. The products can be sustainably obtained, which is highly suitable for industrial applications. ASAA was used to show that $Fe_6Ni_{10}O_x$ is the best catalyst among the investigated Fe-Ni-O_x series with an overpotential of as low as 0.286 V (10 mA cm^{-2}) and a Tafel slope of 48 mV/decade for the electrochemical oxygen evolution reaction. Therefore, this work contributes a versatile, continuous, and reliable way to produce and optimize amorphous metal oxide catalysts.*

Electrochemical water splitting is currently being paid considerable attention, as H_2 is currently produced in industry by the reformation of fossil fuels.[1] The purity of H_2 from water splitting is theoretically 100 %, and no CO_2 is produced. However, trace impurities of CO or S that are formed in traditional methods can poison some catalysts, especially anode Pt catalysts in H_2 fuel cells.[2] Furthermore, large amounts of CO_2 exhaust gases from fossil fuel reformation is contributing to the global warming problem. It is also an efficient way to timely store sustainable but intermittent energy, for example, solar energy.[3] Very recently, Cronin et al. designed a unique electrolysis cell that allows temporally separated O_2 and H_2 evolution by using a phosphomolybdate anion as a redox equivalent.[4] This cell allows the practical utilization the electrolysis to be approached.

The fundamental study of and search for materials for electrochemical water splitting have been significantly developed. For the cathodic H_2 evolution reaction (HER), a few layered MoS_2/WS_2 nanosheets,[5] and Ni_2P nanoparticles[6] have been found to possess good activity as cheaper candidates to replace Pt. The anodic O_2 evolution reaction (OER) associated with four-electron transfer has required more efforts because of its high kinetic barrier and sluggish reaction dynamics. Many metal oxides, hydroxides, and spinel compounds have been identified as efficient OER catalysts in alkaline media.[7] Layered double hydroxides (LDHs),[8] optimized perovskite oxides,[9] and Co-based composite catalysts[10] were extensively studied and have shown excellent performance. Furthermore, amorphous metal oxides have been proven to possess surprising OER performance with lower overpotential and Tafel slope than crystalline oxides.[11] These results have inspired us to look for efficient and reliable ways to search for and identify the best catalysts from the huge groups of amorphous metal oxides. Electrodeposition and newly developed photochemical metal–organic deposition (PMOD)[11c] seem to be the most acceptable methods for accessing amorphous metal oxides. However, the former is always invalid for mixed metal oxides with a precise proportion of various elements, and both of them are not commercially applicable in the scalable production of catalysts or electrodes. Therefore, it is still a challenge to develop a large-scale approach to produce these compounds with the correct elemental proportions and to satisfy the numerous demands for their use as catalysts.

Herein, we report the aerosol-spray-assisted approach (ASAA) as a precisely controllable and successive method to fabricate and optimize amorphous metal oxides with adjustable compositions and mesoporous structures. Although aerosol-spray-assisted evaporation-induced self-assembly (EISA) devices have been developed for preparing mesoporous products,[12] this is the first report to date that systematically confirms this technique as an efficient methodology for accessing amorphous mixed metal oxides for electrochemical applications. The elemental proportion can be accurately controlled from the mother solution and the catalytic performance of the products can be easily engineered. The availability is corroborated through a case study of composite Ni-Fe-O_x catalysts, which were chosen because they are well-studied so that it is easier and more reliable to evaluate this method.[13] By using ASAA, we have shown that the best catalyst of Fe-Ni-O_x is $Fe_6Ni_{10}O_x$, with an overpotential of as low as 0.286 V at 10 mA cm^2 and a Tafel slope of 48 mV/decade. More valuably, this method is suitable for the large-scale industrial production as we can successively obtain products with a rate of about 0.1 g h^{-1} merely from a home-made device.

[*] L. Kuai, J. Geng, C. Chen, E. Kan, Y. Liu, Q. Wang, Prof. Dr. B. Geng
College of Chemistry and Materials Science
The Key Laboratory of Functional Molecular Solids
Ministry of Education
Anhui Laboratory of Molecular-Based Materials
Center for Nano Science and Technology, Anhui Normal University
Wuhu 241000 (P. R. China)
E-mail: bygeng@mail.ahnu.edu.cn

[**] This work was supported by the National Natural Science Foundation of China (21271009), the Program for New Century Excellent Talents in University (NCET 11-0888), the Doctoral Fund of the Ministry of Education of China (20123424110002), the Science and Technological Fund of Anhui Province for Outstanding Youth (1308085JGD01), the Foundation of Key Project of Natural Science of Anhui Education Committee (KJ2012A143) and the Program for Innovative Research Team at Anhui Normal University.

Supporting information for this article is available on the WWW under http://dx.doi.org/10.1002/anie.201404208.

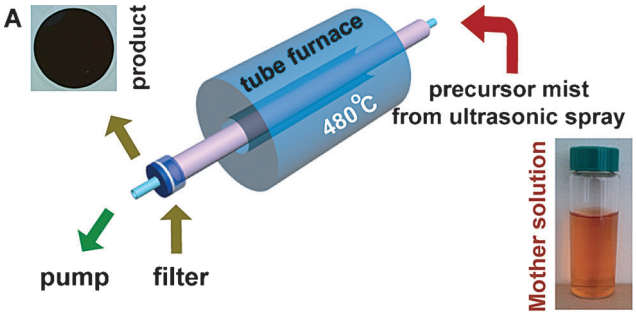

Figure 1. A) Illustration of the setup and processes associated in the ASAA for amorphous metal oxide microspheres; B) highlighted possible amorphous metal oxides that can be obtained from the ASAA with inorganic salts.

Our home-made setup is shown in Figure 1 A (a photograph is given in Figure S1 in the Supporting Information), as well as the associated processes for producing amorphous metal oxide microspheres with mesoporous structures, including three parts of an ultrasonic humidifier for the spraying process, a tube furnace for metal oxide formation and EISA, and a collector for capturing the powders. We take the preparation of Fe-Ni-O_x as an example. Firstly, the ethanolic precursor solution containing Pluronic P123, $Fe(NO_3)_3$ and/or $Ni(NO_3)_2$ salts is sprayed with the assistance of an ultrasonic humidifier. The mist (Figure 1 A, right-hand side) is then driven into the tube furnace (preheated to 480 °C) by a pump (Figure 1 A, left-hand side). During the process in the furnace, which last only a short time (several seconds), precursor inorganic salts in the spray drops are firstly solidified, subsequently decomposed into amorphous metal oxides, and finally assembled with the assistance of the EISA of P123. The short reaction time in the furnace means that the metal oxides do not have sufficient time to crystallize and the final products are amorphous. Figure 1 B highlights the possible metal oxides (single-component or composite oxides) that can be prepared by using the ASAA with inorganic salts. Compared with the costly and time-consuming PMOD route,[11a] this method allows the use of cheap inorganic salts as precursors instead of expensive and water-sensitive metal–organic compounds. More importantly, the reaction can be completed within several seconds, and we can continuously obtain products as soon as the precursors are prepared, which is highly suitable for industrial production. The rate is estimated at about 0.1 g h^{-1} just from a single home-made device. Therefore, this is a versatile and scalable method to search for, study, and produce amorphous metal oxides as OER catalysts and/or cocatalysts for water splitting.

Figure 2 shows the SEM images of eight typical products from ASAA, namely, NiO (A, B), $Fe_1Ni_{10}O_x$ (C, D), $Fe_2Ni_{10}O_x$ (E, F), $Fe_6Ni_{10}O_x$ (G, H), $Fe_{10}Ni_{10}O_x$ (I, J), $Fe_{10}Ni_6O_x$ (K, L), $Fe_{10}Ni_2O_x$ (M, N), and Fe_2O_3 (O, P). The size ranges from 0.2 to 2 μm, which is dictated by the size distribution of the mist drops. The pure NiO products are concave hollow microspheres, while the Fe_2O_3 products are solid microspheres. According to the model of Lenggoro et al.,[14] the reason for this difference may be due to the lower diffusion rate of Ni^{2+} than that of Fe^{3+} during the solidification and decomposition process in the furnace. When the Fe/Ni ratio increases, the morphology tends to pure Fe_2O_3-like, and $Fe_6Ni_{10}O_x$ (see Figure 2 E for a typical case). As shown in Figure S2 (see the

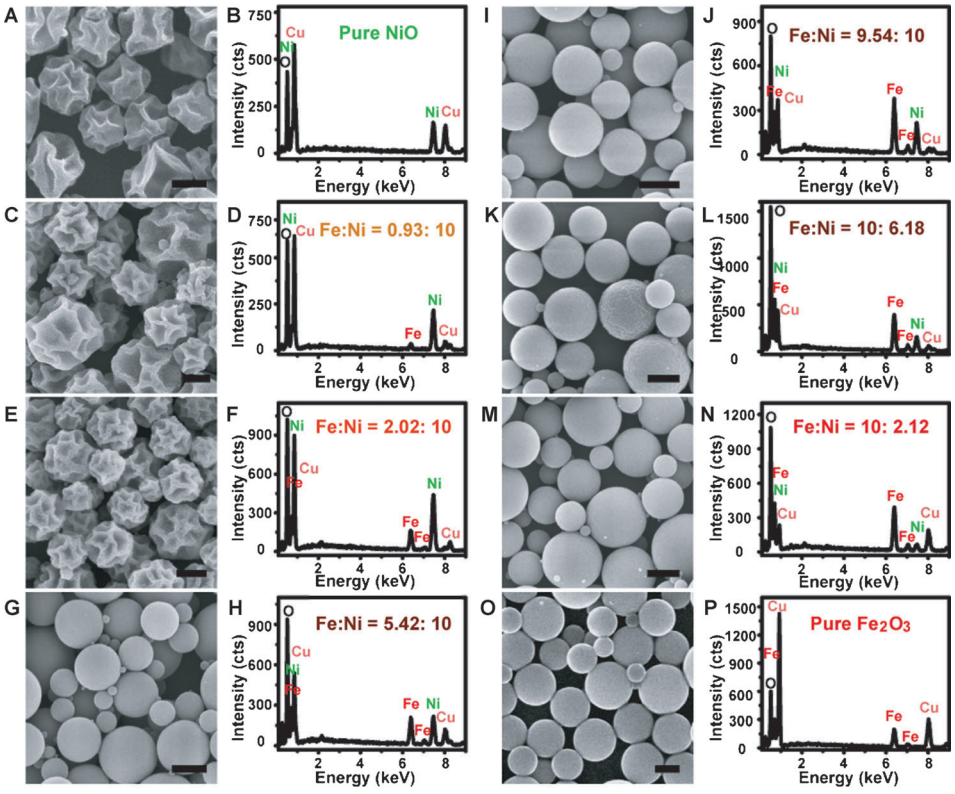

Figure 2. SEM images (first and third rows) and EDX patterns (second and fourth rows) of NiO (A, B), $Fe_1Ni_{10}O_x$ (C, D), $Fe_2Ni_{10}O_x$ (E, F), $Fe_6Ni_{10}O_x$ (G, H), $Fe_{10}Ni_{10}O_x$ (I, J), $Fe_{10}Ni_6O_x$ (K, L), $Fe_{10}Ni_2O_x$ (M, N), and Fe_2O_3 (O, P) microspheres. Scale bars: 500 nm.

Supporting Information), the products are mesoporous structures after removing the P123 template. Energy dispersive X-ray (EDX) spectroscopy analysis was performed to evaluate the availability of this method to accurately control the composition. The peaks representing Cu are from the Cu grid for EDX measurements. No signals corresponding to metallic impurities are observed in the spectra of the single-component NiO and Fe_2O_3. More importantly, the ratios from EDX analysis are very close to the original ratios of the mother solutions for all Fe-Ni-O_x samples to within about 5%. The high accuracy in the control of the contents is attributed to the fast and complete co-decomposition of precursor in the droplet microreactors. Furthermore, this is a versatile approach for the fabrication and surveying of many other amorphous multicomponent metal oxide catalysts with precisely controlled proportions of components, such as Co-Fe-O_x and Co-Ni-O_x (see Figure S3).

EDX spectroscopy was used to verify the uniform elemental distribution of the samples by investigating five random points at the same test grid. Even for the sample with low iron content ($Fe_2Ni_{10}O_x$; Figure S4 in the Supporting Information), the atomic ratio difference is only about 5%, which is very close to the precursor Fe/Ni ratio (1.98). HAADF-STEM-EDX element mapping was carried out to directly determine the distribution of various metal elements. Taking $Fe_6Ni_{10}O_x$ as an example (Figure 3A), the Fe (red), Ni (green), and O (yellow) elements are uniformly distributed in the microspheres. This information suggests that all the components can be uniformly distributed in the overall products, which gives rise to the precise control of catalyst composition. To further confirm the accuracy in composition control and reproducibility of product preparation, we randomly repeated the preparation of $Fe_{10}Ni_6O_x$ sample six times under the same conditions and analyzed the Ni/Fe ratios from EDX data. As shown in Figure 3B and Figure S5, the proportions of the metals in five samples are very close to the original precursor ratio (6.02) with an atomic ratio difference of within less than 5%, although the ratio of one sample shows an atomic ratio difference of more than 10%, which may arise from some accidental error. Overall, ASAA is indeed a reliable method to accurately control the proportion of the components in the product. Moreover, ASAA is not only a route to produce and optimize the amorphous metal oxides, but also a reliable methodology to study and search more efficient electrocatalysts. The precise control of the components means that this method would play an important role in the fundamental study of amorphous catalysts for electrochemical OER. However, the challenge remains that it is difficult to obtain the products with a uniform particle size distribution, which is determined by the spraying process.

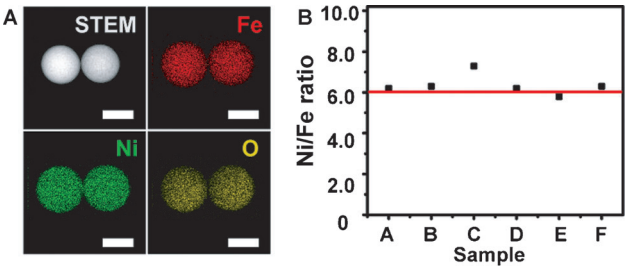

Figure 3. HAADF-STEM-EDX element mapping of Fe_6Ni_{10} (A) and the Ni/Fe proportion statistics of six random $Fe_{10}Ni_6O_x$ samples (B). HAADF = high-angle annular dark-field imaging. Scale bars: 500 nm.

The electrocatalytic water splitting performance of Fe-Ni-O_x catalysts with different Fe/Ni ratios was identified in 1.0 M KOH at room temperature. The pH value of the electrolyte was measured as 13.63. The solution was kept O_2-saturated to maintain the standard balance potential of H_2O/O_2 (1.23 V vs. RHE). All the potentials were iR-compensated (the resistance was read directly from the workstation via AC impedance measurements (iR-drop compensation)). In this work, we studied eight Fe-Ni-O_x samples, which are labeled as follows: NiO, Fe_1Ni_{10}, Fe_2Ni_{10}, Fe_6Ni_{10}, $Fe_{10}Ni_{10}$, $Fe_{10}Ni_6$, $Fe_{10}Ni_2$, and finally Fe_2O_3. The catalyst loading was 0.1 mg cm^{-2}. As shown in Figure S6 (see the Supporting Information), a suitable catalyst loading and pH value are both critical for the performance of materials. Figure 4A shows the cyclic voltammograms (CVs) of eight samples. After Fe is embedded in the NiO matrix, the electrochemical properties change significantly compared with pure NiO. The oxidation peak of Ni^{II} to Ni^{III} is positively shifted, which has been observed and investigated in previous work.[13] However, it is interesting to note that the oxidation peak is separated into two parts when the Fe content is more than 10%. The first peak is close to that of pure NiO while the other peak appears later. Similarly, the electrochemical capacitance varies as the Fe content is changed. In addition, we can find that the electrochemical reaction of Fe_2O_3 is

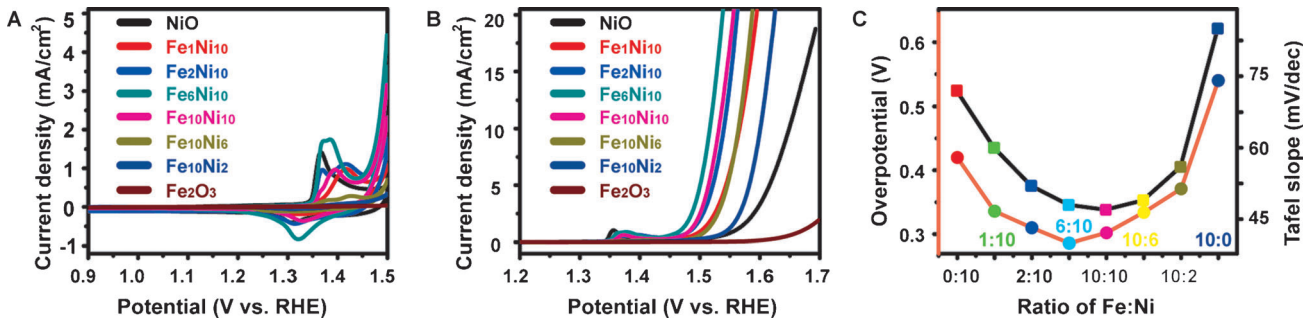

Figure 4. A) CVs, B) LSV curves, overpotential (at 10 mA cm^{-2}), and C) Tafel slope plots of Fe-Ni-O_x catalysts with different Fe/Ni ratios in O_2-saturated 1.0 M KOH solution.

negligible in the studied electrochemical window. However, the electronic structure and corresponding electrochemical nature of NiO is notably changed after the addition of Fe. As a result, the products exhibit distinct electrochemical water-splitting properties (shown in Figure 4B). Obviously, Fe_6Ni_{10} exhibits the best performance with an overpotential of 0.286 V at a current density of 10 mA cm^{-2} and a Tafel slope of 48 mV/decade. Figure 4C summarizes the Fe/Ni ratio-dependent overpotential (at 10 mA cm^{-2}, red curve) and Tafel slope (black curve) of the studied samples. The overpotential for pure Fe_2O_3 is estimated according to its linear sweep voltammetry (LSV) curve. As is clearly shown, the addition of Fe remarkably improves the electrochemical water splitting activity. The overpotential minimum occurs at Fe_6Ni_{10}. Furthermore, when the Fe content is around 50%, the Tafel slope reaches its optimal value (around 48 mV/decade). Moreover, we observe that Fe-Ni-O_x with a higher proportion of Fe shows a lower Tafel slope than those with a lower proportion of Fe. These results are consistent with previously reported pioneering work.[13] Based on the above results and discussion, it can be concluded that the ASAA is a rather efficient and highly reliable approach for accessing and identifying amorphous metal oxide OER catalysts for water splitting, in particular multicomponent species.

We also studied the effect of the crystalline phase change on the electrochemical water-splitting performance. The Fe_6Ni_{10} sample was calcined at 200, 300, 400, and 500 °C. As shown in Figure 5A, crystalline NiO is formed after calcination. The magnetic phase appears at 400 °C, leading to the peak centered at 37° to become asymmetric (Figure S7 in the Supporting Information). A typical $NiFe_2O_4$ phase can be found after calcination at 500 °C. Moreover, the electrochemical properties are apparently changed after calcination. According to the CVs (Figure 5B), the electrochemical capacitance is majorly reduced. It is found that the capacitance falls as the calcination temperature increases. When magnetic $NiFe_2O_4$ is formed after calcination at both 400 and 500 °C, the Faradic capacitance is almost negligible. This information implies that the amorphous mixed metal oxides possess a larger capacitance than crystalline oxides, which may bring some new insight in the material design for electrochemical energy-storage devices. More importantly, the electrochemical water-splitting performance is strongly dependent on the calcination temperature, which affects the charge-storage capacitance. The degree of inhibition of catalytic performance is consistent with the decrease of capacitance of the catalysts. As shown in Figure 5b, about 150 mV more overpotential for both Fe_6Ni_{10}(400°C) and Fe_6Ni_{10}(500°C) is needed to achieve a current density of 10 mA cm^{-2} compared to the original amorphous Fe_6Ni_{10} sample. Hence, the electrochemical capacitance may be one of the important factors or descriptors for electrochemical water splitting. By carefully studying the LSV curves, we see that the metal oxide discharges first before water splitting. After forward discharge, many positive charges are localized in the electrode interface and a corresponding electric field is built up at the same time. The localized electric field pushes the electrons away from OH^- ions so that oxygen molecules are formed. The larger capacitance indicates that a larger area of electric field is built up, so that a better electrochemical water splitting performance is achieved.

In summary, the ASAA is a reliable route to produce, optimize, and study amorphous metal oxide materials, as shown by a case study of Fe-Ni-O_x catalysts. The proportion of the components can be precisely controlled by this method. Furthermore, this method allows the products to be continuously obtained. The best catalyst for electrochemical water splitting among the investigated Fe-Ni-O_x series is $Fe_6Ni_{10}O_x$ with an overpotential of as low as 0.286 V at 10 mA cm^{-2} and a Tafel slope of 48 mV/decade. Therefore, this work will guide us in searching for good catalysts among the huge group of amorphous metal oxides, and is a scalable method for industrial production and commercial applications.

Experimental Section

Synthesis of amorphous Fe-Ni-O_x catalysts: $Fe(NO_3)_3$ and $Ni(NO_3)_2$ (2 mmol in total, with determined ratio), triblock copolymer P123 (0.25 g) were dissolved in absolute ethanol (30 mL). The solution was transferred into a medical-use ultrasonic humidifier (1.7 MHz, 35 W) for the aerosol-spraying process. The generated mist was drawn into a glass tube in a tube furnace (67 cm, preheated to 480 °C) by a vacuum pump. The products were collected on filter paper. The mesoporous products were obtained after washing with ethanol to remove the P123 template. The sample of $Fe_6Ni_{10}O_x$ was calcined at 200, 300, 400, and 500 °C for 4 h in an air atmosphere with a rate of 2 °C min^{-1}. Characterization and electrochemical measurements are given in the Supporting Information.

Received: April 10, 2014
Published online: June 4, 2014

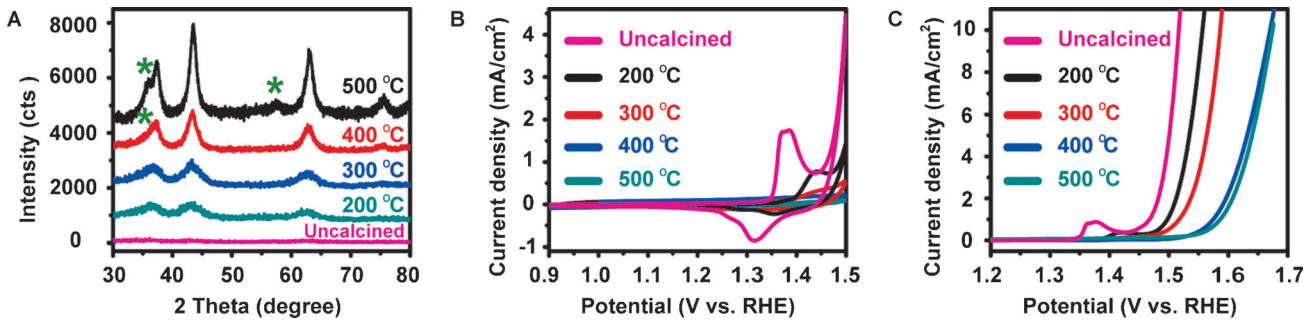

Figure 5. A) XRD patterns, B) CVs, and C) LSV curves of Fe_6Ni_{10} samples in O_2-saturated 1.0 M KOH solution after calcination.

Keywords: aerosol sprays · heterogeneous catalysis · metal oxides · oxygen evolution reaction · water splitting

[1] a) J. D. Holladay, J. Hu, D. L. King, Y. Wang, *Catal. Today* **2009**, *139*, 244; b) L. G. Bloor, P. I. Molina, M. D. Symes, L. Cronin, *J. Am. Chem. Soc.* **2014**, *136*, 3304.
[2] C. L. Spiegel, *Designing & Building Fuel Cells*, McGraw-Hill, New York, **2007**.
[3] A. Vojvodic, J. K. Nørskov, *Science* **2011**, *334*, 1355.
[4] a) M. D. Symes, L. Cronin, *Nat. Chem.* **2013**, *5*, 403; b) T. E. Mallouk, *Nat. Chem.* **2013**, *5*, 362.
[5] a) Y. G. Li, H. L. Wang, L. M. Xie, Y. Y. Liang, G. S. Hong, H. J. Dai, *J. Am. Chem. Soc.* **2011**, *133*, 7296; b) J. F. Xie, H. Zhang, S. Li, R. X. Wang, X. Sun, M. Zhou, J. F. Zhou, X. W. Lou, Y. Xie, *Adv. Mater.* **2013**, *25*, 5807; c) D. Voiry, H. Yamaguchi, J. W. Li, R. Silva, D. C. B. Alves, T. Fujita, M. W. Chen, T. Asefa, V. B. Shenoy, G. Eda, M. Chhowalla, *Nat. Mater.* **2013**, *12*, 850.
[6] E. J. Popczun, J. R. McKone, C. G. Read, A. J. Biacchi, A. M. Wiltrout, N. S. Lewis, R. E. Schaak, *J. Am. Chem. Soc.* **2013**, *135*, 9267.
[7] D. E. Hall, *J. Electrochem. Soc.* **1985**, *132*, 41.
[8] a) M. Gong, Y. Guang Li, H. L. Wang, Y. Y. Liang, J. Z. Wu, J. G. Zhou, J. Wang, T. Regier, F. Wei, H. J. Dai, *J. Am. Chem. Soc.* **2013**, *135*, 8452; b) X. X. Zou, A. Goswami, T. Asefa, *J. Am. Chem. Soc.* **2013**, *135*, 17242.
[9] a) J. Suntivich, K. J. May, H. A. Gasteiger, J. B. Goodenough, Y. Shao-Horn, *Science* **2011**, *334*, 1383.
[10] a) Y. Y. Liang, Y. G. Li, H. L. Wang, J. G. Zhou, J. Wang, T. Regier, H. J. Dai, *Nat. Mater.* **2011**, *10*, 780; b) M.-R. Gao, Y.-F. Xu, J. Jiang, Y.-R. Zheng, S.-H. Yu, *J. Am. Chem. Soc.* **2012**, *134*, 2930; c) M.-R. Gao, X. Cao, Q. Gao, Y.-F. Xu, J. Jiang, S.-H. Yu, *ACS Nano* **2014**, *8*, 3970.
[11] a) M. W. Kanan, D. G. Nocera, *Science* **2008**, *321*, 1072; b) E. Tsuji, A. Imanishi, K.-I. Fukui, Y. Nakato, *Electrochim. Acta* **2011**, *56*, 2009; c) R. D. L. Smith, M. S. Prévot, R. D. Fagan, Z. P. Zhang, P. A. Sedach, M. K. J. Siu, S. Trudel, C. P. Berlinguette, *Science* **2013**, *340*, 60; d) R. D. L. Smith, M. S. Prévot, R. D. Fagan, S. Trudel, C. P. Berlinguette, *J. Am. Chem. Soc.* **2013**, *135*, 11580; e) R. D. L. Smith, B. Sporinova, R. D. Fagan, S. Trudel, C. P. Berlinguette, *Chem. Mater.* **2014**, *26*, 1654.
[12] a) Y. F. Lu, H. Y. Fan, A. Stump, T. L. Ward, T. Rieker, C. J. Brinker, *Nature* **1999**, *398*, 223; b) C.-K. Tsung, J. Fan, N. F. Zheng, Q. H. Qi, A. J. Forman, J. F. Wang, G. D. Stucky, *Angew. Chem.* **2008**, *120*, 8810; *Angew. Chem. Int. Ed.* **2008**, *47*, 8682; c) C. Boissiere, D. Grosso, A. Chaumonnot, L. Nicole, C. Sanchez, *Adv. Mater.* **2011**, *23*, 599; d) D. P. Debecker, M. Stoyanova, F. Colbeau-Justin, U. Rodemerck, C. Boissière, E. M. Gaigneaux, C. Sanchez, *Angew. Chem.* **2012**, *124*, 2171; *Angew. Chem. Int. Ed.* **2012**, *51*, 2129; e) Z. Jin, M. D. Xiao, Z. H. Bao, P. Wang, J. F. Wang, *Angew. Chem.* **2012**, *124*, 6512; *Angew. Chem. Int. Ed.* **2012**, *51*, 6406.
[13] a) D. A. Corrigan, *J. Electrochem. Soc.* **1987**, *134*, 377; b) M. W. Louie, A. T. Bell, *J. Am. Chem. Soc.* **2013**, *135*, 12329.
[14] I. W. Lenggoro, T. Hata, F. Iskandar, M. M. Lunden, K. Okuyama, *J. Mater. Res.* **2000**, *15*, 733.

